# Systemic delivery of siRNA to tumors using a lipid nanoparticle containing a tumor-specific cleavable PEG-lipid

Hiroto Hatakeyama[a,d], Hidetaka Akita[a,d], Erika Ito[a,d], Yasuhiro Hayashi[a,d], Motoi Oishi[b,d], Yukio Nagasaki[c,d], Radostin Danev[e], Kuniaki Nagayama[e], Noritada Kaji[f], Hiroshi Kikuchi[g], Yoshinobu Baba[f], Hideyoshi Harashima[a,d*]

[a] Faculty of Pharmaceutical Sciences, Hokkaido University, Kita-12, Nishi-6, Kita-ku, Sapporo 060-0812, Japan

[b] Tsukuba Research Center for Interdisciplinary Material Science (TIMS), University of Tsukuba, 1-1-1 Ten-noudai, Tsukuba, Ibaraki 305-8573, Japan

[c] Gaduate School of Pure and Applied Sciences, Graduate School of Comprehensive Human Sciences, Satellite Laboratory, Satellite Laboratory, International Center for Materials Nanoarchitectonics (MANA), National Institute of Materials Science (NIMS), University of Tsukuba, 1-1-1 Tennoudai, Tsukuba, Ibaraki 305-8573, Japan

[d] The Core Research for Evolutional Science ant Technology (CREST), Japan Science and Technology Agency (JST), Japan

[e] Okazaki Institute for Integrative Bioscience, 5-1 Higashiyama, Myodaiji-cho, Okazaki, Aichi 444-8787, Japan

[f] Graduate School of Engineering, Nagoya University, Furo-cho, Chikusa-ku, Nagoya, Aichi 464-8603, Japan

[g] Formulation Research Laboratories, Eisai Co. Ltd., Tokodai 5-1-3, Tukuba, Ibaraki 300-2635, Japan

*Corresponding author: Hideyoshi Harashima

Adress: Kita12 Nishi6, Kita-ku, Sapporo, Hokkaido 060-0812, Japan.

Tel: +81-11-706-3919

Fax:+81-11-706-4879

E-mail: harasima@pharm.hokudai.ac.jp

## Abstract

Previously, we developed a multifunctional envelope-type nano device (MEND) for efficient delivery of nucleic acids. For tumor delivery of a MEND, PEGylation is a useful method, which confers a longer systemic circulation and tumor accumulation via the enhanced permeability and retention (EPR) effect. However, PEGylation inhibits cellular uptake and subsequent endosomal escape. To overcome this, we developed a PEG-peptide-DOPE (PPD) that is cleaved in a matrix metalloproteinase (MMP)-rich environment. In this study, we report on the systemic delivery of siRNA to tumors by employing a MEND that is modified with PPD (PPD-MEND). An in vitro study revealed that PPD modification accelerated both cellular uptake and endosomal escape, compared to a conventional PEG modified MEND. To balance both systemic stability and efficient activity, PPD-MEND was further co-modified with PEG-DSPE. As a result, the systemic administration of the optimized PPD-MEND resulted in an approximately 70% silencing activity in tumors, compared to non-treatment. Finally, a safety evaluation showed that the PPD-MEND showed no hepatotoxicity and innate immune stimulation. Furthermore, in a DNA microarray analysis in

liver and spleen tissue, less gene alternation was found for the PPD-MEND compared to that for the PEG-unmodified MEND due to less accumulation in liver and spleen.

*Keywords:* Multifunctional envelope-type nano device (MEND); systemic siRNA delivery; cleavable PEG; Matrix Metalloproteinase; PEG dilemma; EPR effect

## 1. Introduction

The passive tumor targeting of liposomes is achieved through the enhanced permeability and retention (EPR) effect [1,2]. To produce liposomes that have a long circulation time, they are generally modified by poly(ethylene glycol) (PEG) and the product is referred to as a "stealth liposome" [3,4]. Stealth liposomes are used in clinical applications to deliver doxorubicin (Doxil) in the treatment of the acquired immunodeficiency syndrome (AIDS)-related Koposi's sarcoma [5].

However, PEGylation hampers in vivo applications of nanoparticles that are intended for use for the delivery of nucleic acids, such as plasmid DNA (pDNA) and small interfering RNA (siRNA). From the view point of nucleic acid delivery, it is necessary that nucleic acids arrive at an intracellular organelle for successful functioning (e.g. cytosol for siRNA, nucleus for pDNA) [6]. However, PEGylation inhibits the intracellular trafficking of nanoparticles, especially in cellular uptake and subsequent endosomal escape leading to significant loss of activity [7,8], which is referred to as the "PEG dilemma" [9].

To solve this, cleavable PEG systems that are removed in response to intracellular environments such as the low pH in endosomes/lysosomes and thiolytical molecules have been proposed [10-15]. Specific environments in tumor tissues

have been also utilized as a trigger for PEG cleavage [16-20]. We constructed a tumor specific PEG system in which the PEG is removed by cleavage in the presence of a matrix metalloproteinase (MMP) [17]. MMPs are abundantly distributed in tumor tissue and play a key role in progress and metastasis [21]. A PEG-peptide-dioleoylphosphatidyl ethanolamine (DOPE) ternary conjugate (PPD) containing a peptide sequence that is sensitive to MMP-2 was synthesized. We recently developed a multifunctional envelope-type nano device (MEND), in which nucleic acids are condensed using a polycation to form a core particle that is encapsulated in a lipid envelope for use as a novel non-viral nucleic acid delivery system [22,23]. PPD modified MEND encapsulating pDNA showed enhanced transfection activity in tumors after systemic administration in tumor-bearing mice compared to conventional PEG modified MEND [17].

In the present study, we report on the systemic delivery of siRNA to tumors using a PPD modified MEND. A schematic diagram of the strategy employed is shown in Fig. 1. We tested whether PPD modification improved the intracellular trafficking of the MEND compared to conventional PEG-modified MEND in in vitro experiments. We then optimized the PPD modified MEND for in vivo siRNA delivery through the optimization of PPD modification, in which a combination of

PEG-DSPE was used to achieve stability in systemic circulation and activity in tumor tissue. We evaluated the PPD modified MEND for its safety in cytokine studies and using a DNA microarray in the form of toxicogenomics studies [24].

## 2. Material and methods

### 2.1 Materials

Anti-luciferase siRNA (21-mer, 5'-GCGCUGCUGGUGCCAACCCTT-3', 5'-GGGUUGGCACCAGCAGCAGCGCTT-3'), anti-green fluorescent protein (GFP) siRNA (21-mer, 5'-GCUGACCCUGAAGUUCAUCTT-3', GAUGAACUUCAGGGUCAGCTT-3') and the matrix metalloproteinase cleavable peptide (sequence: GGGVPLSLYSGGGG) were obtained from Thermo Electron GmbH (Ulm, Germany). DOPE, 1,2-dioleoyl-3-trimethylammonium-propane (DOTAP), cholesterol, distearoyl-*sn*-glycero-3-phoshoethanolamine-N-[methoxy (polyethylene glycol)-2000] ($PEG_{2k}$-DSPE), $PEG_{5k}$-DSPE, 7-nitrobenz-2-oxa-1,3-diazole labeled DOPE (NBD-DOPE) and rhodamine labeled DOPE (Rho-DOPE) were purchased from AVANTI Polar Lipids (Alabaster, AL, USA). Stearyl octaarginine (STR-R8) was obtained from KURABO INDUSTRIES (Osaka, Japan). PEG-peptide-DOPE (PPD) was synthesized as described previously [17]. RiboGreen and Lysotracker Green were purchased from Molecular Probes (Eugene, OR, USA). Alexa488-tagged siRNA and Alelx546-tagged siRNA was purchased from QIAGEN (Hilden, Germany). Luciferase assay reagents and reporter lysis buffer were obtained from Promega

(Madison, WI, USA). [$^3$H]cholesteryl hexadecyl ether (CHE), Soluene-350 and Hionic Fluor were purchased from Perkin-Elmer Life Sciences Japan (Tokyo, Japan). ELISA assay kits of Quantikine Immunoassay mouse IL-6 and TNF-α were purchased from R&D systems (Minneapolis, MN, USA). Transaminase CII-test WAKO was obtained from Wako (Osaka, Japan).

### 2.2 Experimental animals

Male ICR mice (5-6 weeks old) and male BALB/c nude mice (5-6 weeks old) were purchased from CLEA (Tokyo, Japan). Tumor-bearing mice were prepared by the subcutaneous injection of male BALB/c nude mice with HT1080-luc cells ($10^6$ cells/mouse). All *in vivo* experiments were approved by the Institutional Animal Care and Use Committee.

### 2.3 Cell culture

HT1080 cells stably expressing luciferase (HT1080-luc) were cultured in cell-culture dishes (Corning) containing culture medium supplemented with 10% fetal bovine serum, penicillin (100 U/ml), streptomycin (100 μg/ml), G418 (0.4 mg/ml) at 37°C in an atmosphere of 5% $CO_2$ and 95% humidity.

## 2.4 Preparation of MENDs

siRNA (0.1 mg per ml) was complexed with STR-R8 (0.1 mg per ml), at a nitrogen/phosphate ratio of 1.0, in 250 μl of hepes buffer. A lipid film was formed by evaporating a chloroform solution containing DOTAP, DOPE and cholesterol (125 nmol total lipids in 3:4:3 molar ratio). The lipid films for the MENDs modified with PEG-DSPE and PPD were prepared by evaporation using predetermined amounts of PEG-DSPE and PPD. The siRNA/STR-R8 complex was applied to the lipid film, followed by incubation for 10 min at room temperature to permit the lipids to become hydrated. To coat the siRNA/STR-R8 complex with the lipid, the lipid film was then sonicated for approximately 1 min in a bath-type sonicator. The average diameter and the ζ-potential of the condensed siRNA and MENDs were determined using a Zetasizer Nano ZS ZEN3600 (MALVERN Instrument, Worchestershire, UK). siRNA recovery ratio was determined using a RiboGreen assay, comparing fluorescence (excitation: 480 nm, emission: 520 nm) in the presence and absence of polyaspartic acid and Triton X-100, as described previously [25].

### 2.5 Electron microscopy of PEGylated MENDs

To visualize MEND modified with 15 mol% $PEG_{2k}$-DSPE ($PEG_{2k}$-MEND) and MEND modified with 11.25 mol% PPD and 3.75 mol% $PEG_{5k}$-DSPE (PPD/$PEG_{5k}$-MEND), Rho-DOPE (0.5 mol% of total lipids) labeled MENDs containing Alexa488-tagged siRNA were layered on a discontinuous sucrose density gradient (0–60%), and centrifuged at 160,000 g for 2 h at 20 °C. Aliquots (1 ml) were collected from the top, and the fluorescent intensity of rhodamine (excitation: 576 nm, emission: 597 nm) and Alexa488 (excitation: 495 nm, emission: 519 nm) was measured in each fraction. Fractions containing both rhodamine and Alexa488 were used as the purified PEGylated MEND. A suspension of the purified MEND was placed on a copper grid coated with a carbon film. After carefully removing any excess liquid with the tip of a filter paper, the sample was rapidly frozen in liquid ethane using a Leica rapid-freezing device (Leica EM CPC system). The grid, with ice-embedded samples, was transferred to the specimen chamber of a transmission electron microscope using a cryo-transfer system. The specimen chamber was cooled with liquid helium to reduce damage to the specimen by the electron beam. For observations, a JEOL JEM-3100FFC electron microscope with an HDC phase plate inserted into the

back focal plane of the objective lens was operated at 300 kV [26,27].

### 2.6 *In vitro* silencing activity of MENDs

To examine the *in vitro* silencing effect of the MENDs, $4\times10^4$ HT1080-luc cells were seeded in a 24-well dish one day prior to transfection. MENDs, containing 2.4 μg of siRNA, were added to 0.25 ml of culture medium containing 10% serum, followed by incubation at 37 °C for 3 hr. Then, 0.75 ml of culture medium containing 10% serum was added to the cells, followed by incubation at 37 °C for 21 hr. The cells were washed with 0.5 ml PBS and lysed with reporter lysis buffer. Luciferase activity in cell lysates was then measured using a luminometer (Luminescencer-PSN, ATTO, Japan). Protein concentrations were determined using a BCA Protein Assay Kit (Pierce, Rockford, IL). Luciferase activity is expressed as relative light units (RLU) per mg of protein. The silencing effect was calculated as a percentage using the following equation:

$$\text{silencing effect (\%)} = \left(1-\frac{TE_{anti-luc}}{TE_{anti-GFP}}\right)\times100$$

where $TE_{anti\text{-}luc}$ and $TE_{anti\text{-}GFP}$ represent luciferase gene expression after transfection with either anti-luciferase siRNA or anti-GFP siRNA, respectively. We confirmed that the anti-GFP siRNA used in this study has no effect on

luciferase expression by comparison with non-treatment cells.

### 2.6 Quantification of cellular uptake of MENDs

To examine the *in vitro* cellular uptake of the MENDs, $2.5\times10^5$ HT1080-luc cells were seeded in a 6-well dish one day prior to transfection. MENDs labeled with 0.5 mol% NBD-DOPE, containing 7.2 μg siRNA, was added to 1 ml of culture medium containing 10% serum, followed by incubation at 37 °C for 2 hr. The cells were washed three times with 1 ml PBS supplemented heparin (20 units/ml) to remove surface bound MENDs. The cells then were washed with 1 ml of Krebs Ringer solution and were observed by flow cytometry (FACScan, Becton Dickinson).

### 2.7 Quantitative evaluation of endosomal escape of PEGylated MENDs by confocal images

To evaluate the endosomal escape of PEGylated MENDs, quantification of the confocal images was done using a confocal image-assisted three dimensionally integrated quantification (CIDIQ) method [28]. One day prior to observation, $2.5\times10^5$ HT1080-luc cells were seeded in a glass-base dish (IWAKI, Chiba, Japan).

PEGylated MENDs containing 7.2 μg Alexa546 labeled siRNA, were incubated with cells at 37 °C for 3 hr. To stain endosomes/lysosomes, the cells were incubated with 10 μM Lysotracker Green for 30 min. The cells were then washed three times with 1 ml PBS supplemented heparin (20 units/ml) to remove the surface bound PEGylated MENDs. Twenty Z-series images of the cells were obtained from top-to-bottom using a LSM 510 META (Carl Zeiss Co. Ltd., Jena, Germany) confocal laser scanning microscope equipped with an oil-immersion objective lens (Plan-Apochromat 63×/NA =1.4). Each 8-bit TIFF image was transferred to Image Pro Plus ver.4.0 (Media Cybernetics Inc., Silver Spring, MD, USA) to quantify the total brightness and pixel area of each r.o.i. For the data analysis, the pixel areas of each cluster in the endosome/lysosome: $s_i$(end/lys) and cytosol $s_i$(cyt) were separately summed in each X-Y plane, and are denoted as $S_z$ =$J$(end/lys) and $S_z$=$J$(cyt), respectively. The values for $S_z$=$J$(end/lys) and $S_z$=$J$(cyt) in each X-Y plane were further summed through all the Z-series of images, and are denoted as $S$(end/lys) and $S$(cyt), respectively. These values represent the total amount of siRNA in the endosoms/lysosomes and the cytosol in an individual cell. The fraction of siRNA in the cytosol to that totally introduced on $F$(cyt), were calculated as follows:

$F(\mathrm{cyt}) = S(\mathrm{cyt})/(S(\mathrm{end/lys}) + S(\mathrm{cyt}))$.

### 2.8 *In vivo* systemic stability and biodistribution of MENDs

To evaluate the systemic stability and biodistribution of MENDs, the lipid envelope of MENDs were labeled with [$^3$H]CHE [29]. The MENDs were administered to male ICR mice via the tail vein, at a dose of 80 μg of siRNA. At the indicated times post-injection, radioactivity in the blood was measured as described previously [30]. Briefly, at the indicated times, the mice were sacrificed and blood was collected. A 100 μl sample of blood was solubilized in 1 ml of Soluene-350 for 1 hr at 40 °C, and the solution then decolorized by the treatment with $H_2O_2$. Radioactivity was determined by liquid scintillation counting, after adding 10 ml of Hionic fluor. The blood concentration is represented as the %ID per ml of blood. To evaluate the biodistribution in tumor bearing mice, MENDs labeled with [$^3$H]CHE at a dose of 80 μg of siRNA were injected via the tail vein into tumor-bearing mice with tumor sizes of 300-500 mm$^3$. After 24 hr, the tumor, liver and spleen were collected and the radioactivity was then determined as described previously [30]. Tissue accumulation of MENDs is represented as the %ID per g of tissue.

### 2.9 *In vivo* silencing activity of PEGylated MEND in tumor tissue

PEGylated MENDs were injected into tumor-bearing mice via the tail vein at a dose of 80 μg siRNA. As 24 hr post-injection, the tumors were excised and homogenized in reporter lysis buffer (1 ml) using a POLYTRON homogenizer (KINEMATICA). The resulting tumor homogenate was centrifuged at 15000 rpm for 10 min at 4 °C to obtain the supernatant. The luciferase activity of the supernatant (20 μl) was assayed using the Luciferase Assay System and the results are expressed as relative light units (RLU) per g of tumor.

### 2.10 Histological observation

$PEG_{2k}$-MEND and PPD/$PEG_{5k}$-MEND labeled with Rho-DOPE at a dose of 80 μg siRNA were injected via the tail vein into tumor bearing mice with tumor sizes of 300-500 $mm^3$. At 6 hr post-injection, the tumors were excised, and embedded in OCT compound (Sakura Fine Technical, Tokyo, Japan) and snap-frozen in liquid nitrogen. Frozen samples were cut in 10 μm-thick sections (LEICA CM3000, Leica Microsystems, Wetzlar, Germany). Epidermal growth factor receptor (EGFR) was immunolabeled with an anti-EGFR antibody (1:500 dilution; Abcam, Tokyo,

Japan) overnight at 4 °C, followed by the treatment with a Alexa488-labeled anti-rat IgG antibody (1:1000; Invitrogen, Carlsbad, CA, USA) for 1 hr at room temperature. The samples were observed using a LSM 510 META microscope equipped with an objective lens (Plan-Apochromat 20×/NA =1.4).

### 2.11 Determination of serum level of ALT and cytokines

MENDs at a dose of 80 μg of siRNA were injected via the tail vein into male ICR mice, and blood was collected at the indicated times. Hepes-buffered glucose (HBG) treatment was used as a control. A hydrodynamics-based injection was performed according to the method of Liu et al [31]. Briefly, 2 ml of saline was injected via the tail vain within 5 s. Poly IC at a dose of 80 μg in HBG was injected via tail vein. Blood samples were stored overnight at 4°C, followed by centrifugation (10000 rpm, 4 °C, 10 min) to obtain serum. ALT levels in serum were measured with test kits, and IL-6 and TNF-α levels in serum were determined with ELISA kits according to the manufacturer's instructions.

### 2.12 DNA microarray analysis

Either PEG-unmodified MEND or PPD/$PEG_{5k}$-MEND was administered to male

ICR mice via the tail vein, at a dose of 80 μg of siRNA. HBG treatment was used as a control. At 2 hr after injection, liver and spleen tissues were collected, and stored in RNAlater solution at -20 °C to avoid RNA degradation. Liver and spleen samples were homogenized and total cellular RNA was purified using an RNeasy mini kit, as described above. Total RNA extracted from four mice spleens (125 ng each) were pooled into one sample (total 500 ng) for normalizing individual differences. The integrity of the pooled total RNA samples was evaluated using an Agilent 2100 Bioanalyzer (Agilent, Foster City, CA, USA). The pooled RNA was labeled with Cy3 or Cy5 using the Low RNA Input Fluorescent Linear Amplification Kit (Product No. 5184-3568), followed by purification using an RNeasy mini kit to eliminate unlabeled RNA. Cy3-labeled HBG and Cy5-labeled MEND (or PPD/$PEG_{5k}$-MEND) cRNA sample was then hybridized to Agilent Whole Mouse Genome Microarray (Product No. G4122A) according to manufacturer's hybridization instruction. These experimemts were carried out in duplicate using exchanged dye-labeled cRNA probes (i.e., Cy3 and Cy5 dye-swapping experiments). The microarray slides were analyzed using an Agilent Microarray scanner (Product No. G2565AA). Microarray expression data were obtained using the Agilent Feature Extraction software (Version A.6.1.1).

### 2.13 Statistical analysis

Comparisons between multiple treatments were made using one-way analysis of variance (ANOVA), followed by the Dunnett test. Pair-wise comparisons between treatments were made using a student's t-test. A $P$-value of $< 0.05$ was considered significant.

## 3. Results

### 3.1 Characteristics of the prepared MENDs

The average diameter and ζ-potential of siRNA complexed with STR-R8 were approximately 70 nm and -20 mV, respectively. The average diameters and ζ-potentials of the prepared MENDs that were used in the in vitro and in vivo experiments are summarized in Table 1 and Table 2, respectively. The PEG-unmodified MEND (MEND) had a diameter of 180 nm, and was positively charged due to the presence of the cationic lipid. The inversion of ζ-potential indicates that the siRNA complex was encapsulated by the lipid envelope. Five mol% of $PEG_{2k}$-DSPE or PPD-modification reduced the diameter and the positive charge was decreased compared to the MEND because the surface of the lipid envelope was masked by the aqueous layer of the PEG moiety (Table 1). The sizes and ζ-potentials of the PEG-MEND and PPD-MEND were comparable, suggesting that particles with a similar morphology had been prepared. For in vivo experiments, the MEND was modified with 15 mol% of PEG-lipid, which resulted in particles with a diameter of 80~110 nm and a ζ-potential of -5 ~ -12 mV, respectively (Table2). Quantification of siRNA complex in the lipid envelope was performed using RiboGreen as described previously [25]. The result of this test

suggested that approximately 70% of the total siRNA complex was confined within the lipid envelope. As shown in Fig. 2, the electron micrograph of a MEND modified with 15 mol% $PEG_{2k}$-DSPE ($PEG_{2k}$-MEND) and a MEND modified with 11.25 mol% PPD and 3.75 mol% $PEG_{5k}$-DSPE (PPD/$PEG_{5k}$-MEND) revealed the PEGylated MEND particles were spherical, with a diameter of approximately 100 nm, which is consistent with the diameters measured by a Zetasizer (Table 2).

### 3.2 Effect of PPD modification on in vitro silencing activity, uptake and endosomal escape

To evaluate the utility of PPD, we initially performed in vitro experiments using MENDs modified with $PEG_{2k}$-DSPE (PEG-MEND) or PPD (PPD-MEND) at 5 mol% of the total lipid in HT1080-luc cells. The peptide sequence in PPD is sensitive to MMP-2 and MMP-9 [32]. The MMP-2 concentration in the culture medium of HT1080 was sufficient to cleave the 5 mol% of PPD on the surface of the MEND, as demonstrated previously [17,33]. Findings related to the silencing activity of MENDs are shown in Fig. 3A. In contrast to the high silencing activity observed for the PEG-unmodified MEND (MEND), the PEG-MEND showed no silencing activity. However, when the $PEG_{2k}$-DSPE was replaced with PPD, the

silencing activity of the MEND was enhanced. To determine whether the enhanced silencing activity of PPD-MEND was the result of improved intracellular trafficking, we investigated the cellular uptake and subsequent endosomal escape of MENDs using flow cytometory and confocal laser scanning microscopy. While the amount of PEG-MEND taken up was decreased to around 20% compared to MEND, the use of the PPD-MEND resulted in a recovery of up to around 60% (Fig.3 B).

We also quantitatively compared endosomal escape between PEG-MEND and PPD-MEND using the CIDIQ method [28]. Cells were treated with PEGylated MENDs loaded with Alexa-546 labeled siRNA, and the endosomes/lysosomes fraction was then stained with Lysotracker Green at 2.5 hr post-transfection. A Z-series of images were then captured by confocal laser scanning microscopy (Fig.4A and B for PEG-MEND and PPD-MEND, respectively). siRNA signals colocalized with Lysotracker Green (yellow clusters) are denoted as siRNAs in endosomes/lysosomes. The siRNA signals that were not colocalized with Lysotracker Green (red clusters) are denoted as those that escaped from endosomes/lysosomes. For quantification, the pixel areas of the siRNA clusters detected in the cytosol (red clusters) and in endosomes/lysosomes (yellow clusters)

were separately integrated through all of the Z-series of images. The calculation for PEG-MEND in 24 individual cells indicated an average endosomal escape efficiency of 33.6%. On the other hand, that obtained from PPD-MEND in 24 individual cells indicated an escape efficiency of 70.5%. These results suggest that the enhanced silencing activity of the PPD-MEND was achieved through an enhanced cellular uptake and accelerated endosomal escape compared to the PEG-MEND.

### 3.3 in vivo optimization of PEG-DSPE and PPD on the systemic circulation

For in vivo applications of MENDs in tumor delivery, sufficient systemic stability is required to result in the efficient tumor accumulation of MENDs via the EPR effect. As demonstrated previously, the long blood circulation of MEND in which the lipid envelope was composed of DOTAP, DOPE and cholesterol, was achieved by modification with 15 mol% $PEG_{2k}$-DSPE [17]. In contrast to $PEG_{2k}$-DSPE, the half life in the blood of the 15 mol% PPD modified MEND was inadequate after i.v. injection, presumably because the PEG moiety of PPD was displayed as an inappropriate form in circulating blood. We demonstrated that a combination of PPD and either $PEG_{2k}$-DSPE or $PEG_{5k}$-DSPE is needed to fulfill both long

circulation and in vivo activity. The MEND was modified with various proportions of PPD and PEG-DSPE, in which total PEG-lipid was fixed at 15 mol% of the total lipid, and the blood concentration was evaluated at 6 hr after i.v. injection into mice. In the combination of PPD and $PEG_{2k}$-DSPE, the PEGylated MEND retained systemic stability up to a ratio of 50% of PPD (7.5 mol% of PPD and 7.5 mol% $PEG_{2k}$-DSPE) as shown in Fig.5. On the other hand, a high systemic stability was found for the PEGylated MEND with a 75% of PPD ratio in combination with $PEG_{5k}$-DSPE (11.25 mol% of PPD and 3.75 mol% of $PEG_{5k}$-DSPE). The following in vivo studies were performed using a MEND modified with 11.25 mol% PPD and 3.75 mol% $PEG_{5k}$-DSPE as PPD/$PEG_{5k}$-MEND.

### 3.4 Biodistribution analysis of MENDs in tumor bearing mice

We next evaluated the biodistribution of a PEG-unmodified MEND (MEND), a MEND modified with $PEG_{2k}$-DSPE ($PEG_{2k}$-MEND) and a PPD/$PEG_{5k}$-MEND in tumor bearing mice. As shown in Fig. 6, the MEND disappeared from the blood by 6hr after i.v. injection, due to clearance by the liver and spleen, which resulted in poor tumor accumulation. In contrast to the MEND, the $PEG_{2k}$-MEND and the

PPD/$PEG_{5k}$-MEND showed a longer blood circulation time, due to less clearance by the liver and spleen, leading to tumor accumulation via the EPR effect. These results suggest that a PPD modified MEND could reach in vivo tumor tissue after systemic administration.

### 3.4 In vivo silencing activity of PEGylated MENDs in tumor bearing mice

The in vivo silencing activity of PEGylated MENDs was evaluated in tumor-bearing mice after i.v. injection. Because the PEG-unmodified MEND did not accumulate, it was excluded from the in vivo silencing test. While the $PEG_{2k}$-MEND showed no silencing activity, sufficient knockdown of luciferase activity (approximately 70% v.s. NT) was observed in tumor tissues that had been treated with the PPD/$PEG_{5k}$-MEND (Fig. 7). We additionally determined the silencing activity of a MEND modified with 7.5 mol% of PPD and $PEG_{2k}$-DSPE (PPD/$PEG_{2k}$-MEND). The silencing activity of the PPD/$PEG_{2k}$-MEND was determined to be approximately 35%.

### 3.5 Histological observation of PEGylated MENDs in tumor

We determined the distribution of PEGylated MENDs labeled with rhodamine in

tumor tissue in the following experiments. After preparing 10 μm-thick sections of tumor tissue in which human EGF receptor was immunestained with green fluorescence as a tumor marker, samples were observed by confocal laser scanning microscopy. Red signals, denoting $PEG_{2k}$-MEND or PPD/$PEG_{5k}$-MEND were broadly detected inside tumor cells as shown in Fig. 8. These results suggested that, because tumor accumulation and the cellular uptake of the $PEG_{2k}$-MEND and the PPD/$PEG_{5k}$-MEND appeared to be nearly comparable, the in vivo enhanced silencing activity of the PPD/$PEG_{5k}$-MEND can be attributed to an efficient endosomal escape.

### 3.6 Safety evaluation of MENDs in vivo

As shown in Fig. 6, the major organs for clearing the systemically administered MENDs are reticuloendothelial systems (RES), such as the liver and spleen [34]. We therefore observed the hepatotoxicity of MENDs. At 24 hr after i.v. administration, neither the MEND, the $PEG_{2k}$-MEND nor the PPD/$PEG_{5k}$-MEND had an influence on serum ALT levels comparable to HBG treatment, as shown in Fig. 9A. On the other hand, the significant increase in serum ALT level caused by a hydrodynamics-based injection as positive control, indicates that MENDs have

no hepatotoxicity after systemic administration. We then investigated the innate immune stimulation of MENDs over 24 hr. As previous reports, serum levels of IL-6 and TNF-α are frequently employed as an index of an innate immune response and systemic inflammation after i.v. injections of lipoplexes and polyplexes [35-38]. As shown in Fig. 9B, C, treatment with poly IC resulted in the production of IL-6 and TNF-α, and the MEND stimulated the innate immune system to a sight degree. On the other hand, after the administration of the $PEG_{2k}$-MEND and the PPD/$PEG_{5k}$-MEND, these cytokine levels were equal to that observed as the result of an HBG treatment. Based on these results, PPD and PEG-DSPE modified MENDs containing siRNA do not appear to have any effect on the innate immune response.

### 3.7 Microarray analysis of MEND

However, biochemical tests such as ALT and certain cytokine analyses (Fig. 9) provide only limited information regarding biological reactions after the systemic administration of a gene carrier. To understand what occurs in a host following the systemic administration of MENDs, hepatic and splenic gene expression profiles in mice that had been treated with the PEG-unmodified MEND (MEND)

and the PEGylated MEND (PPD/$PEG_{5k}$-MEND) were generated using whole genome oligonucleotide microarrays. The liver and spleen are the main clearance organs, and the spleen is the largest secondary lymphoid organ associated with an immune response [39]. Mice were injected via the tail vein with HBG, the MEND or the PPD/$PEG_{5k}$-MEND. After 2 hr, the livers and spleens were collected and RNA was prepared. Microarrays were then hybridized as described in Materials and Methods. Using a 2-fold change relative to the HBG treatment as a criterion for differential expression, 7 and 21 genes were extracted from the administration of MEND, which are shown in order of magnitude of altered expression levels by the MEND treatment compared with HBG for the liver and spleen, respectively (Fig. 10 and Table 3). The up-regulated genes are classified as interferon related genes (4 genes in the liver and 12 genes in the spleen), oligoadenylated synthetases (1 and 6 genes) and heat shock proteins (2 and 3 genes). As shown in Table 3, the ratios of PEGylated MEND/MEND indicate values of less than 1, indicating that PEGylation reduced biological reactions to the systemically administered MENDs containing siRNA.

## Discussion

The findings reported herein demonstrate the utility of tumor specific cleavable PEG for the systemic delivery of siRNA to tumor by means of a MEND. As a proof-of-concept experiment, we analyzed the intracellular trafficking of a PPD modified MEND in cultured cells. In an in vitro experiment, the MEND was modified with either 5 mol% $PEG_{2K}$-DSPE (PEG-MEND) or PPD (PPD-MEND). As shown in Table 1, PPD modification shielded the surface positive charge as well as the PEG-MEND. In contrast to the PEG-unmodified MEND, the PEG-MEND showed no silencing effect due to the inhibition of cellular uptake (Fig. 3) or endosomal escape (Fig. 4). These are recognized as main processes to be considered in the "PEG dilemma" [9]. Modification of the MEND with PPD improved these steps. The concentration of MMP-2 in the HT1080 medium was sufficient to digest the peptide in PPD at 5 mol% on the surface of the MEND as demonstrated previously [17,33]. The removal of the PEG moiety from the surface of the MEND allowed the MEND to associate with the cell surface via electrostatic interactions, followed by endocytosis mediated cellular uptake. The endosomal escape of a lipid based nanoparticle is mediated by membrane fusion with an endosomal membrane [40]. PEGylation solidly stabilizes the lipid lamellae

structure of nanoparticles, which inhibits the disruption of the lamellae structure, thus allowing fusion with the endosomal membrane [40,41]. Therefore, PPD cleavage also contributes to an enhanced endosomal escape by promoting the disruption of the lipid envelope and membrane fusion with endosomes. Based on these results, it appears that a PPD cleavable system is a potential strategy for the efficient delivery of siRNA to the cytosol in tumor cells.

For the in vivo delivery of a MEND to tumors via the EPR effect, a long systemic circulation time is required. Unexpectedly, the modification of PPD alone was not sufficient to enhance the systemic stability of the MEND, as shown in Fig. 5. One possible reason is that the peptide in PPD is digested by serum enzymes during circulation in the blood. The other is that, since the peptide sequence in PPD has hydrophobic properties (hydropathy index; 3.3, [42]), the peptide might associate with the lipid membrane, which would decrease the flexibility of PEG, resulting in an inappropriate form of PEG, such as a pancake form, leading to less blood circulation [4,43]. To improve the systemic stability of the PPD modified MEND, we partially replaced PPD with PEG-DSPE at various ratios where the amount of PEG-lipid was fixed at 15 mol% of the total lipid. It was reported that the combination of different lengths of PEG chains prolonged the blood circulation

time of PEGylated liposomes [44]. Therefore, we also examined the effect of a longer PEG chain with a molecular weight of 5000 ($PEG_{5k}$-DSPE) on the systemic stability of a PPD modified MEND. In the case of the combination of $PEG_{2K}$-DSPE, the stability of the PPD modified MEND, up to a PPD ratio of 50%, was comparable to that for a MEND modified only with $PEG_{2K}$-DSPE. The PPD modified MEND with $PEG_{5K}$-DSPE exhibited a high systemic stability up to a ratio of 75 % PPD. These results suggest that the combination of PPD with $PEG_{5K}$-DSPE achieved a cleavable area accounting for 75% on the surface of MEND. It is likely that the presence of PEG-DSPE blocks the association of the peptide in PPD with the lipid envelope, which results in a PEG moiety with a more flexible form in PPD, such as a mushroom or brush structure, thus extending the circulation time. These findings point to a possibly reason for why the stability of PPD is inferior to PEG-DSPE. It is possible that PPD is not digested by enzymes in the serum, but represents an inappropriate form of PEG due to the hydrophobic property in the peptide.

The in vivo silencing activity of the PEGylated MEND was reflected in the fraction of PPD (Fig. 7), which would result from the cleavage of PPD in response to MMP in a tumor. The concentration of MMP-2 was determined to be

approximately 4 and 0.4 ng/mg protein in vitro HT1080-luc cells and in vivo tumor tissue, respectively, as determined by enzyme-linked immunosorbent assay (ELISA). Typically, $4\times10^4$ cells are cultured in 500 μl of medium. On the other hand, in the in vivo tumor tissue, 1 g of tissue contains approximately $1\times10^8$ cells, which are surrounded by 200 μl of extracellular space [45]. Therefore, the in vivo extracellular space per cell is $6.25\times10^3$ times higher than in vitro culture medium per cell. Calculations indicate that the extracellular concentration of MMP-2 in the in vivo tumor is $6.25\times10^2$ times higher than that of the in vitro culture medium. Unlike culture medium, MMP is assumed to be highly concentrated in the lean extracellular space. As a result, its concentration is sufficient to catalyze the cleavage of PPD even when PPD is modified at 11.25 mol% in in vivo tumor tissue [17]. Further histological observations revealed that the magnitude of intracellular signals seem to be equivalent in both the conventional PEG-MEND and the cleavable PPD-MEND in tumor tissue (Fig. 8). These findings suggest that the amount of cellular uptake for these MENDs is comparable and that endosomal escape constitutes the more likely step for explaining the PEG dilemma in in vivo tumors. As demonstrated above, for the successful delivery of siRNA to a tumor, a delicate balance between stability in the systemic circulation

and the silencing activity of the delivery system is needed.

On the other hand, the application of siRNA in clinical use requires not only effective but also safe delivery systems. We assessed the hepatotoxicity and innate immune stimulation of the MENDs. Both PEG-unmodified and PEGylated MENDs showed no or negligible hepatotoxicity and innate immune stimulation (Fig. 9). However, examining the production of certain types of cytokines is not sufficient to guarantee the safety of a systemic siRNA delivery system. To address this issue, gene expression profiling represents a promising approache to understanding the underlying mechanism of host responses by delivery systems, in the form of toxicogenomics studies [46-49]. However, the response of a host to a systemically administrated non-viral gene vector has not been examined using this approach. We recently conducted a DNA microarray based analysis of the host response to a systemically administered MEND encapsulating pDNA core [24]. In this study, we performed a DNA microarray-based analysis for the systemically administrated PEG-unmodified MEND and PPD/$PEG_{5K}$-MEND in the liver and spleen. The liver and spleen are main clearance organs for systemically administrated lipid nanoparticles, and the spleen is the largest secondary lymphoid organ and contains tissue macrophages that are associated

with an immune response after an intravenous injection of a lipoplex [39]. The microarray study revealed that 7 and 21 genes were up-regulated in the liver and spleen after an i.v. injection of the PEG-unmodified MEND (Fig. 10 and Table 3). It is known that an immune response to siRNA is mediated by the Toll-like receptors 3 and 7 in endosomes, and depends on the base sequence in the siRNA, followed by the production of inflammatory cytokines and type I IFN [50-52]. The up-regulation of interferon associated genes is consistent with an siRNA mediated innate immune response. The family of 2'-5' oligoadenylated synthetases (OAS) and 2'-5' OAS like proteins are induced by interferon [53]. Heat shock proteins (HSP) also involve with double stranded RNA-dependent protein kinase (PKR) [54]. While further studies will clearly be required to completely understand the mechanisms and pathways for the immune response, a microarray study elucidates the host response to MENDs that contain siRNA. The results also indicate that PPD and PEG-DSPE modification reduced the host response to the MEND in the liver and spleen due to a lowered level of accumulation.

## 5. Conclusion

The findings reported herein show that a tumor specific cleavable PEG (PPD) modified MEND can be used to successfully deliver siRNA to a tumor. The in vitro studies demonstrated that the enhanced silencing activity of the PPD-MEND is the result of an improved intracellular trafficking in uptake and endosomal escape compared to the PEG-MEND. In the in vivo study, an optimization was performed through combining PEG-DSPE to satisfy a balance between a long circulation time and silencing activity. As a result, the PPD modified MEND accumulated in tumors via the EPR effect and exhibited efficient silencing activity. Safety evaluations by means of not only a cytokine study but also a microarray suggest that MENDs are not hepatotoxic and do not stimulate the innate immune system, and that PPD modification provided biocompatibility. The PPD modified MEND represents a promising system for use in the in vivo delivery of siRNA to tumors.

## Acknowledgments

This study was supported in part by Grants-in-Aid for Young Scientists (B) and by Grant for Industrial Technology Research from New Energy and Industrial Technology Development Organization (NEDO). We thank M. S. Feather for his helpful advice in writing the English manuscript.

## References


[1] Matsumura Y, Maeda H. A new concept for macromolecular therapeutics in cancer chemotherapy: mechanism of yumoritropic accumulation of proteins and the antitumor agent smancs. Cancer Res 1986;46:6387-6392.

[2] Maeda H, Sawa T, Konno T. Mechanism of tumor targeted delivery of macromolecular drugs, including the EPR effect in solid tumor and clinical overview of the prototype polymeric drug SMANCS. J Control Release 2001;74:47-61.

[3] Allen TM, Cullis PR. Drug delivery systems: entering the mainstream. Science 2004;303:1818-1822.

[4] Immordino ML, Dosio F, Cattel L. Stealth liposomes: review of the basic science, rationale, and clinical applications, existing and potential. Int J Nanomedicine 2006;1:297-315.

[5] Harrington KJ, Mohammadtaghi S, Uster PS, Glass D, Peters M, Vile RG, et al. Effective Targeting of solid tumors in patients with locally advanced cancers by radiolabeled pegylated liposomes. Clin Cancer Res 2001;7:243-254.

[6] Khalil IA, Kogure K, Akita H, Harashima H. Uptake pathways and subsequent intracellular trafficking in nonviral gene delivery. Pharmacol Rev 2006;58:32-45.

[7] Mishra S, Webster P, Davis ME. PEGylation significantly affects cellular uptake and intracellular trafficking of non-viral gene delivery particles. Eur J Cell Biol 2004;83:97-111.

[8] Remaut K, Lucas B, Braeckmans K, Demeester J, de Smedt SC. Pegylation of liposomes favours the endosomal degradation of the delivered phosphodiester oligonucleotides. J Control Release 2007;117:256-266.

[9] Hatakeyama H, Akita H, Harashima H. A multifunctional envelope type nano device (MEND) for gene delivery to tumours based on the EPR effect: A strategy for overcoming the PEG dilemma. Adv Drug Deliv Rev in press.

[10] Choi JS, MacKay JA, Szoka Jr FC. Low-pH-sensitive PEG-stabilized plasmid-lipid nanoparticles: preparation and characterization. Bioconjugate Chem. 2003;14:420-429.

[11] Shin J, Shum P, Thompson DH. Acid-triggered release via

dePEGylation of DOPE liposomes containing acid-labile vinyl ether PEG-lipids. J Controlled Release 2003;91:187-200.

[12] Nie Y, Günther M, Gu Z, Wagner E. Pyridylhydrazone-based PEGylation for pH-reversible lipopolyplex shielding. Biomaterials 2011;32:858-869.

[13] Dong L, Xia S, Wu K, Hunag Z, Chen H, Chen J, Zhang J. A pH/enzyme-responsive tumor-specific delivery for doxorubicin. Biomaterials 2010;31:6309-6316.

[14] Kirpotin D, Hong K, Mullah N, Papahadjopoulos D, Zalipsky S. Liposomes with detachable polymer coating: destabilization and fusion of dioleoylphosphatidylethanolamine vesicles triggered by cleavage of surface-grafted poly(ethylene glycol). FEBS Lett 1996;388:115-118.

[15] Kuai R, Yuan W, Qin Y, Chen H, Tang J, Yuan M, et al. Efficient delivery of payload into tumor cell in a controlled manner by TAT and thiolytic cleavable PEG co-modified liposomes. Mol Pharm 2010;7:1816-1826.

[16] Terada T, Mizobata M, Kawakami S, Yamashita F, Hashida M. Optimization of tumor-selective targeting by basic fibroblast growth factor-binding peptide grafted PEGylated liposomes. J Control Release

2007;119:262-270.

[17] Hatakeyama H, Akita H, Kogure K, Oishi M, Nagasaki Y, Kihira Y, et al. Development of a novel systemic gene delivery system for cancer therapy with a tumor-specific cleavable PEG-lipid. Gene Ther 2007;14:68-77.

[18] Harris TJ, von Maltzahn G, Derfus AM,Ruoslahti E, Bhatia SN. Proteolytic actuation of nanoparticle self-assembly. Angew Chem Int Ed 2006;45:3161-3165.

[19] Mok H, Bae KH, Ahn CH, Park TG. PEGylation and MMP-2 specifically dePEGylated quantum dots: comparative evaluation of cellular uptake. Langmuir 2009;25:1645-1650.

[20] Lee ES, Na K, Bae YH. Polymeric micelle for tumor pH and folate-mediated targeting. J Control Release 2003;91:103-113.

[21] Egeblad M, Werb Z. New functions for the matrix metalloproteinases in cancer progression. Nat Rev Cancer 2002;2:161-174.

[22] Kogure K, Moriguchi R, Sasaki K, Ueno M, Futaki S, Harashima. Development of a non-viral multifunctional envelope-type nano device by a novel lipid film hydration method. J Control Release 2004;98:317-323.

[23] Kogure K, Akita H, Harashima H. Multifunctional envelope-type nano

device for non-viral gene delivery: concept and application of Programmed Packaging. J Control Release 2007;122:246-251.

[24] Hatakeyama H, Ito E, Yamamoto M, Akita H, Hayashi Y, Kajimoto K, et al. A DNA microarray based analysis of the host response to a non-viral gene carrier: a strategy for improving the immune response. Mol Ther in press.

[25] Heyes J, Palmer L, Bremner K, MacLachlan I. Cationic lipid saturation influences intracellular delivery of encapsulated nucleic acids. J Control Release 2005;107:276-287.

[26] Ohta A, Danev R, Nagayama K, Mita T, Asakawa T, Miyagishi S. Transition from nanotubes to micelles with increasing concentration in dilute aqueous solution of potassium N-acyl phenylalaninate. Langmuir 2006;22:8472-8477.

[27] Masuda T, Akita H, Niikura K, Nishio T, Ukawa M, Enoto K, et al. Envelope-type lipid nanoparticles incorporating a short PEG-lipid conjugate for improved control of intracellular trafficking and transgene transcription. Biomaterials 2009;30:4806-4814.

[28] Akita H, Ito R, Khalil IA, Futaki S, Harashima H. Quantitative

three-dimensional analysis of the intracellular trafficking of plasmid DNA transfected by a nonviral gene delivery system using confocal laser scanning microscopy. Mol Ther 2004;9:443-451.

[29] Stein Y, Halperin G, Stein O. Biological stability of [3H]cholesteryl oleyl ether in cultured fibroblasts and intact rat. FEBS Lett 1980;111: 104-106.

[30] Hatakeyama H, Akita H, Maruyama K, Suhara T, Harashima H. Factor governing the in vivo tissue uptake of transferring coupled polyethylene glycol liposomes in vivo. Int J Pharm 2004;281:25-33.

[31] Liu F, Song Y, Liu D. Hydrodynamics-based transfection in animals by systemic administration of plasmid DNA. Gene Ther 1999;6:1258-1266.

[32] Turk BE, Huang LL, Piro ET, Cantley LC. Determination of protease cleavage site motifs using mixture-based oriented peptide libraries. Nat Biotechnol 2001;19:661-667.

[33] Hatakeyama H, Ito E, Akita H, Oishi M, Nagasaki Y, Futaki S, Harashima H. A pH-sensitive fusogenic peptide facilitates endosomal escape and greatly enhances the gene silencing of siRNA-containing nanoparticles in vitro and in vivo. J Control Release 2009;139:127-132.

[34] Scherphof GL, Dijkstra J, Spanjer HH, Derksen JTP, Roerdink FH. Uptake and intracellular processing of targeted and nontargeted liposomes by rat Kupffer cells in vivo and in vitro. Ann NY Aca Sci 1985;446:368-384.

[35] Zhao H, Hemmi H, Akira S, Cheng SH, Scheule RK, Yew NS. Contribution of Toll-like receptor 9 signaling to the acute inflammatory response to nonviral vectors. Mol Ther 2004;9:241-248.

[36] Yasuda K, Ogawa Y, Yamane I, Nishikawa M, Takakura Y. Macrophage activation by a DNA/cationic liposome complex requires endosomal acidification and TLR9-dependent and -independent pathways. J Leukoc Biol 2005;77:71-79.

[37] Kawakami S, Ito Y,Charoensit P, Yamashita F, Hashida M. Evaluation of proinflammatory cytokine production induced by liner and branched polyethylenimine/plasmid DNA complex in mice. J Pharmcol Exp Ther 2006;317:1382-1390.

[38] Sakurai H, Sakurai F, Kawabata K, Sasaki T, Koizumi N, Huang H, et al. Comparison of gene expression efficiency and innate immune response induced by Ad vector and lipoplex. J Control Release

2007;117:430-437.

[39] Cesta MF. Normal structure, function, and histology of the spleen. Toxicol Ppathol 2006;34:455-465.

[40] Hafez IM, Cullis PR. Roles of lipid polymorphism in intracellular delivery. Adv Drug Deliv Rev 2001;47:139-148.

[41] Li W, Szoka FC Jr. Lipid-based nanoparticles for nucleic acid delivery. Pharm Res 2007;24:438-449.

[42] Kyte J, Doolittle RF. A simple method for displaying the hydropathic character of a protein. J Mol Biol 1982;157:105-132.

[43] Allen TM. The use of glycolipids and hydrophilic polymers in avoiding rapid uptake of liposomes by the mononuclear phagocyte system. Adv Drug Deliv Rev 1994;13:285-309.

[44] Sadzuka Y, Nakade A, Hirama R, Miyagishima A, Nozawa Y, Hirota S, et al. Effects of mixed polyethyleneglycol modification on fixed aqueous layer thickenss and antitumor activity of doxorubicin containing liposome. Int J Pharm 2002;238:171-180.

[45] Tsuji A, Yoshikawa T, Hishide K, Minami H, Kimura M, Nakashima E, et al. Physiologicallyl based pharmacokinetics model for beta-lactam

antibiotics I: Tissue distribution and elimination in rats. J Pharm Sci 1983;72:1239-1252.

[46] Omidi Y, Hollins AJ, Benboubetra M, Drayton R, Benter IF, Akhtar S. Toxicogenomics of non-viral vectors for gene therapy: a microarray study of lipofectin- and oligofectamine-induced gene expression changes in human epithelial cells. J Drug Target 2003;11:311-323.

[47] Omidi Y, Hollins AJ, Drayton RM, Akhtar S. Polypropylenimine dendrimer-induced gene expression changes: the effect of complexation with DNA, dendrimer generation and cell type. J Drug Target 2005;13:431-443.

[48] Tagami T, Hirose K, Barichello JM, Ishida T, Kiwada H. Global gene expression profiling in cultured cells is strongly influenced by treatment with siRNA-cationic liposome complexes. Pharm Res 2008;25:2497-2504.

[49] Beyerle A, Irmler M, Beckers J, Kissel T, Stoeger T. Toxicity pathway focused gene expression profiling of PEI-based polymers for pulmonary applications. Mol Pharm 2010;7:727-737.

[50] Kawai T, Akira S. The role of pattern-recognition receptors in innate immunity: update on Toll-like receptors. Nat Immunol 2010;11:373-384.

[51] Hornung V, Guenthner-Biller M, Bourquin C, Ablasser A, Schlee M, Uematsu S, et al. Sequence-specific potent induction of IFN-alpha by short interfering RNA in plasmacytoid dendritic cells through TLR7. Nat Med 2005;11:263-270.

[52] Judge AD, Sood V, Shaw JR, Fang D, McClintock K, MacLachlan I. Sequence-dependent stimulation of the mammalian innate immune response by synthetic siRNA. Nat Biotechnol 2005;23,457-462.

[53] Hovanessian AG. On the discovery of interferon-inducible, double-stranded RNA activated enzymes: the 2'-5'oligoadenylate synthetases and the protein kinase PKR. Cytokine Growth Factor Rev 2007;18:351-361.

[54] Frémont M, Vaeyens F, Herst CV, De Meirleir KL, Englebienne P. Double-stranded RN-dependent protein kinase (PKR) is a stress-responsive kinase that induces NF-κB-mediated resistance against mercury cytotoxicity. Life Sci 2006;78:1845-1856.

# Figure Captions

**Figure 1 A schematic diagram of the strategy for the systemic delivery of siRNA to tumors by the PPD modified MEND**

PPD modified MEND accumulates in tumor via the EPR effect. MMP is abundantly secreted from tumor cells, which digests the peptide in the PPD. The PEG is then detached from the surface of the MEND, which allows MEND to associate with the tumor cell surface, followed by cellular uptake by endocytosis. The MEND escapes from endosome via membrane fusion, and finally the siRNA complex is delivered into the cytosol.

**Figure 2 Electron micrograph of PEGylated MEND.**

(A), (B) represent electron micrograph of $PEG_{2k}$-MEND and PPD/$PEG_{5k}$-MEND, respectively. Bars indicate 100 nm.

**Figure 3 Silencing activity and cellular uptake of MENDs in vitro**

(A) HT1080-luc cells were transfected with MEND, PEG-MEND or PPD-MEND. Luciferase activity was measured 24 hr after transfection. The RNAi effect was calculated by normalization to cells treated with non-specific (anti-GFP) siRNA. The RNAi effect is expressed as the mean ± SD (n=3). (B) HT1080-luc cells were incubated with MEND, PEG-MEND or PPD-MEND labeled with NBD-DOPE for 2 hr. Then, the cellular

uptake amount of MENDs was determined by flow cytometric analysis. In the bar graph, the relative mean fluorescent intensity was shown as the mean± SD (n=3).

**Figure 4 Endosomal escape efficiency of PEGylated MENDs**

PEG-MEND and PPD-MEND prepared with Alexa546-labeled siRNA were transfected into HT1080-luc cells. The endosomes/lysosomes were stained with Lysotracker green to discriminate between siRNA in endosomes/lysosomes and the cytosol. The fraction of siRNA in endosomes and the cytosol was quantified based on the pixel area of clusters in each region of interest, as described in Methods. (A)(B) Typical confocal images of intracellular trafficking of PEG-MEND (A) or PPD-MEND (B). Green, red and yellow represents endosomes/lysosomes, siRNA in the cytoplasm and siRNA in endosomes/lysosomes, respectively. Bars represent 10 μm. (C) Quantitative comparison of endosome escape efficiency between PEG-MEND and PPD-MEND. Endosome escape efficiency in 24 individual cells was plotted. Bars represent the average values.

**Figure 5 Blood concentration of MENDs modified with PPD and PEG-DSPE.**

Open triangles and closed squares indicate the blood concentration of MENDs modified with PPD and either $PEG_{2k}$-DSPE or $PEG_{5k}$-DSPE at 6 hr after systemic administration to mice. Total amount of PEG-lipid was fixed at 15 mol% of total lipid. % of PPD means the proportion of PPD in PEG-lipid (e.c.; 50% of PPD

means that MEND modified with 7.5 mol% PPD and 7.5 mol% PEG-DSPE). The blood concentration is represented as %ID/ml of blood. Data are represented by the mean ± SD (n=3). ***P*<0.01 vs. MEND modified with PEG-DSPE (0% of PPD) determined by one-way ANOVA followed by Dunnett test.

**Figure 6 Biodistribution of MENDs in tumor-bearing mice**

The biodistribution of PEG-unmodified MEND (MEND), MEND modified with 15 mol% $PEG_{2k}$-DSPE ($PEG_{2k}$-MEND) and MEND modified with 11.25 mol% of PPD and 3.75 mol% of $PEG_{5k}$-DSPE (PPD/$PEG_{5k}$-MEND). Blood concentration at 6 and 24 hr, and tissue distribution at 24 hr after systemic administration of MENDs to tumor-bearing mice are represented by %ID/ml and %ID/g tissue (the mean ± SD, n=3), respectively. ***P*<0.01 vs. PEG-unmodified MEND (MEND) determined by one-way ANOVA followed by Dunnett test.

**Figure 7 Silencing activity of PEGylated MENDs in tumor tissue**

Luciferase activity in tumor tissue at 24 hr after the systemic administration of either MEND modified with 15 mol% $PEG_{2k}$-DSPE ($PEG_{2k}$-MEND), MEND modified with 7.5 mol% PPD and 7.5 mol% of $PEG_{2k}$-DSPE (PPD/$PEG_{2k}$-MEND) or MEND modified with 11.25 mol% of PPD and 3.75 mol% of $PEG_{5k}$-DSPE (PPD/$PEG_{5k}$-MEND) is shown as RLU/g tumor. Data are represented as the mean ± SD (n=6). **P*<0.05 and ***P*<0.01 vs. non-treated tumors (NT), as determined by one-way ANOVA followed by Dunnett test.

**Figure 8 Histological observation of PEGylated MENDs in a tumor**

Histological observations were performed using 10 μm-thick tumor sections (A) non-treated or treated with either (B) MEND modified with 15 mol% $PEG_{2k}$-DSPE ($PEG_{2k}$-MEND) or (C) MEND modified with 11.25 mol% of PPD and 3.75 mol% of $PEG_{5k}$-DSPE (PPD/$PEG_{5k}$-MEND). PEGylated MENDs labeled with rhodamine were detected as red signals. Epidermal growth factor receptor (EGFR) was immunolabeled with an anti-EGFR antibody, followed by a Alexa488-labeled secondary antibody. The bars indicate 100 μm.

**Figure 9 Safety evaluation of MENDs**

(A) Hepatotoxicity was evaluated by measuring serum ALT values at 24 hr after the systemic administration of either the PEG-unmodified MEND (MEND), the MEND modified with 15 mol% $PEG_{2k}$-DSPE ($PEG_{2k}$-MEND) or the MEND modified with 11.25 mol% of PPD and 3.75 mol% of $PEG_{5k}$-DSPE (PPD/$PEG_{5k}$-DSPE). A h hydrodynamic injection was performed by the i.v. injection of 2 ml of saline within 5 s. (B)(C) The innate immune response to the MENDs and polyIC was evaluated by determining serum IL-6 and TNF-α values at the indicated times after the systemic administration of MENDs and polyIC. Data are represented as the mean ± SD (n=3).

**Figure 10 Relative gene expression in response to MEND and PPD/$PEG_{5k}$-MEND in the liver and**

**spleen, as determined by a DNA microarray**

Bars represent relative transcriptional levels in (A) liver and (B) spleen from the microarray analysis after MEND and PPD/$PEG_{5k}$-MEND treatment. Numbers in x-axis represent individual gene corresponds to the numbers in Table 3.

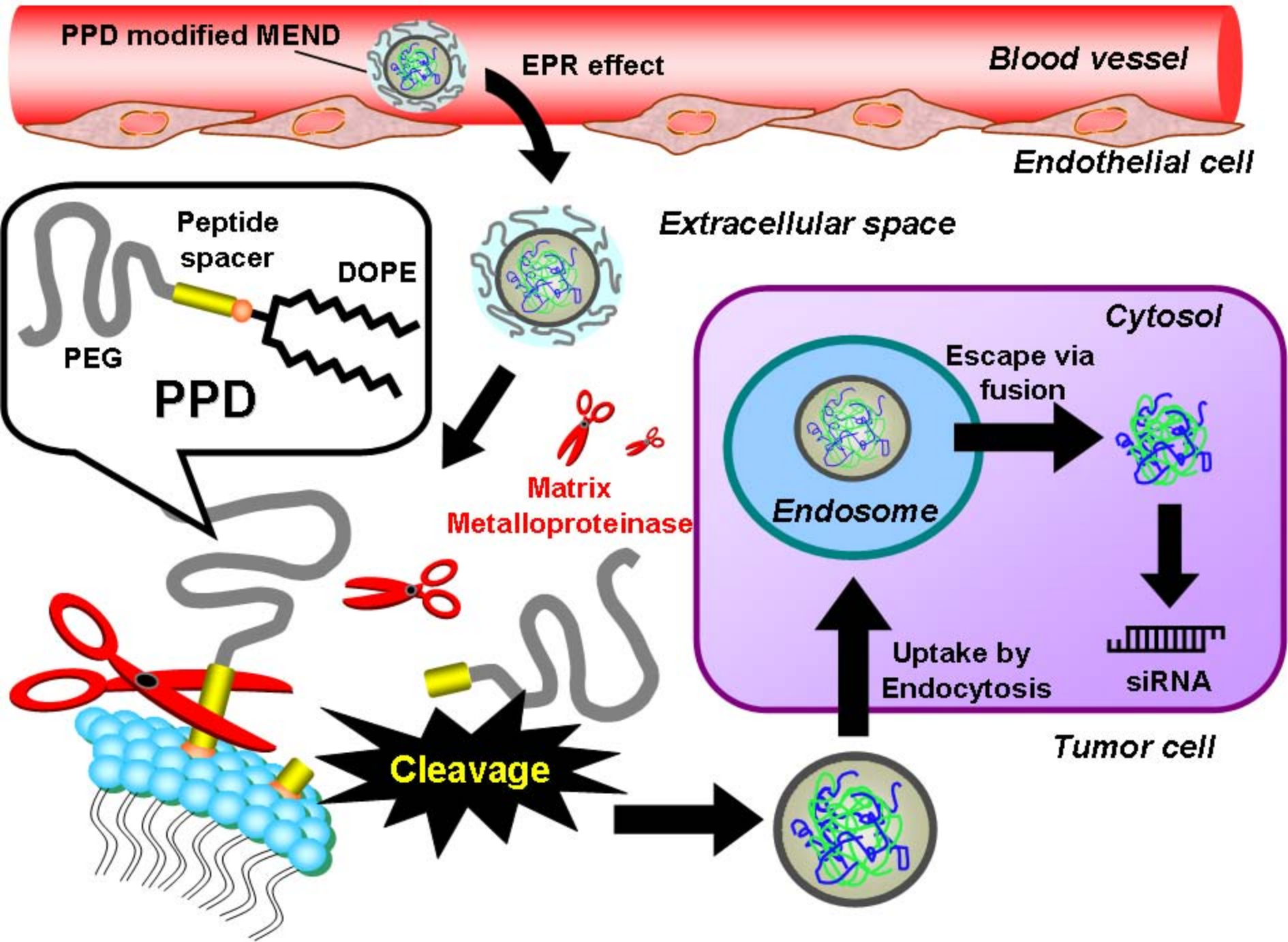
PPD modified MEND
EPR effect
Blood vessel
Endothelial cell
Extracellular space
Peptide spacer
DOPE
PEG
PPD
Matrix Metalloproteinase
Cytosol
Escape via fusion
Endosome
siRNA
Uptake by Endocytosis
Tumor cell
Cleavage

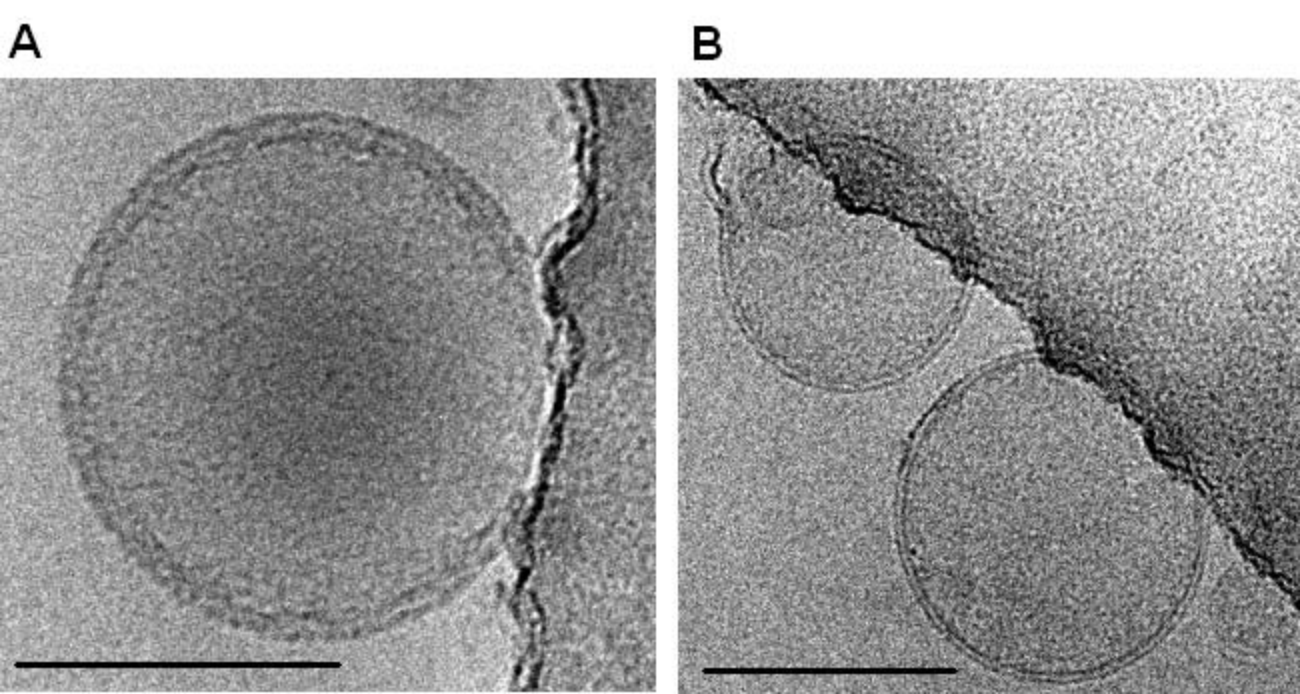
A
B

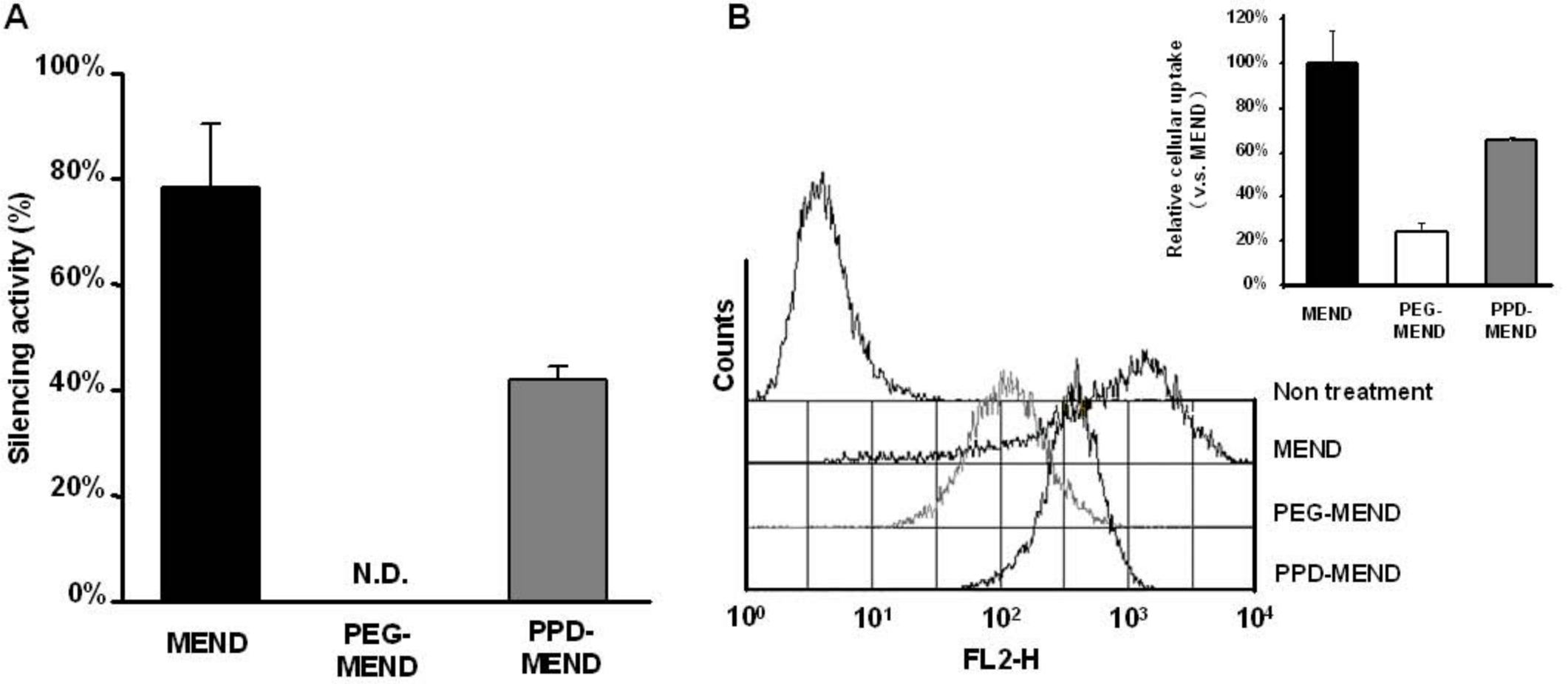
A
100%
80%
60%
40%
20%
0%
Silencing activity (%)
N.D.
MEND
PEG-MEND
PPD-MEND
B
120%
100%
80%
60%
40%
20%
0%
Relative cellular uptake (v.s. MEND)
MEND
PEG-MEND
PPD-MEND
Counts
Non treatment
MEND
PEG-MEND
PPD-MEND
10^0
10^1
10^2
10^3
10^4
FL2-H

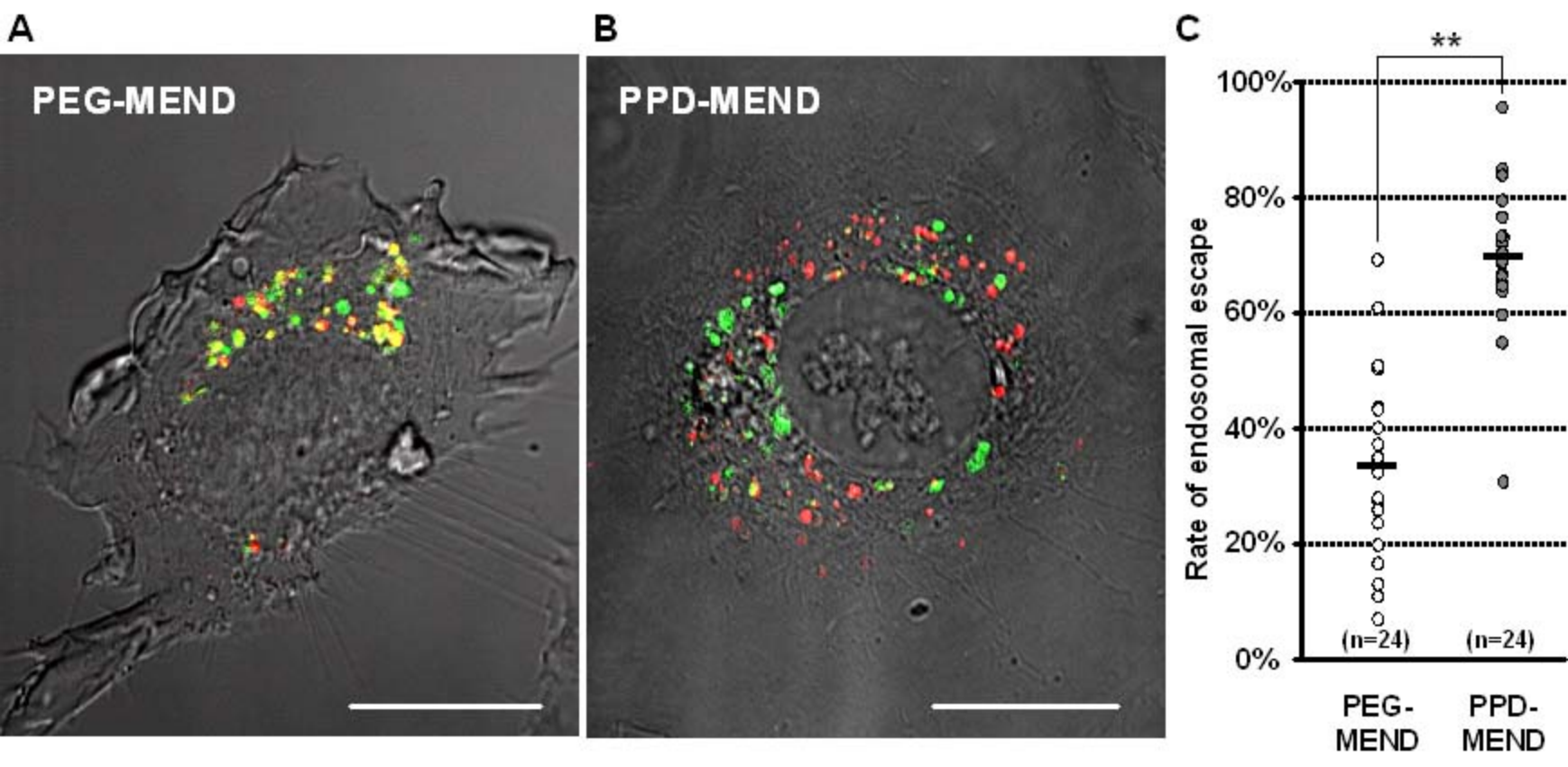
A
PEG-MEND
B
PPD-MEND
C
**
100%
80%
60%
40%
20%
0%
Rate of endosomal escape
(n=24)
(n=24)
PEG-MEND
PPD-MEND

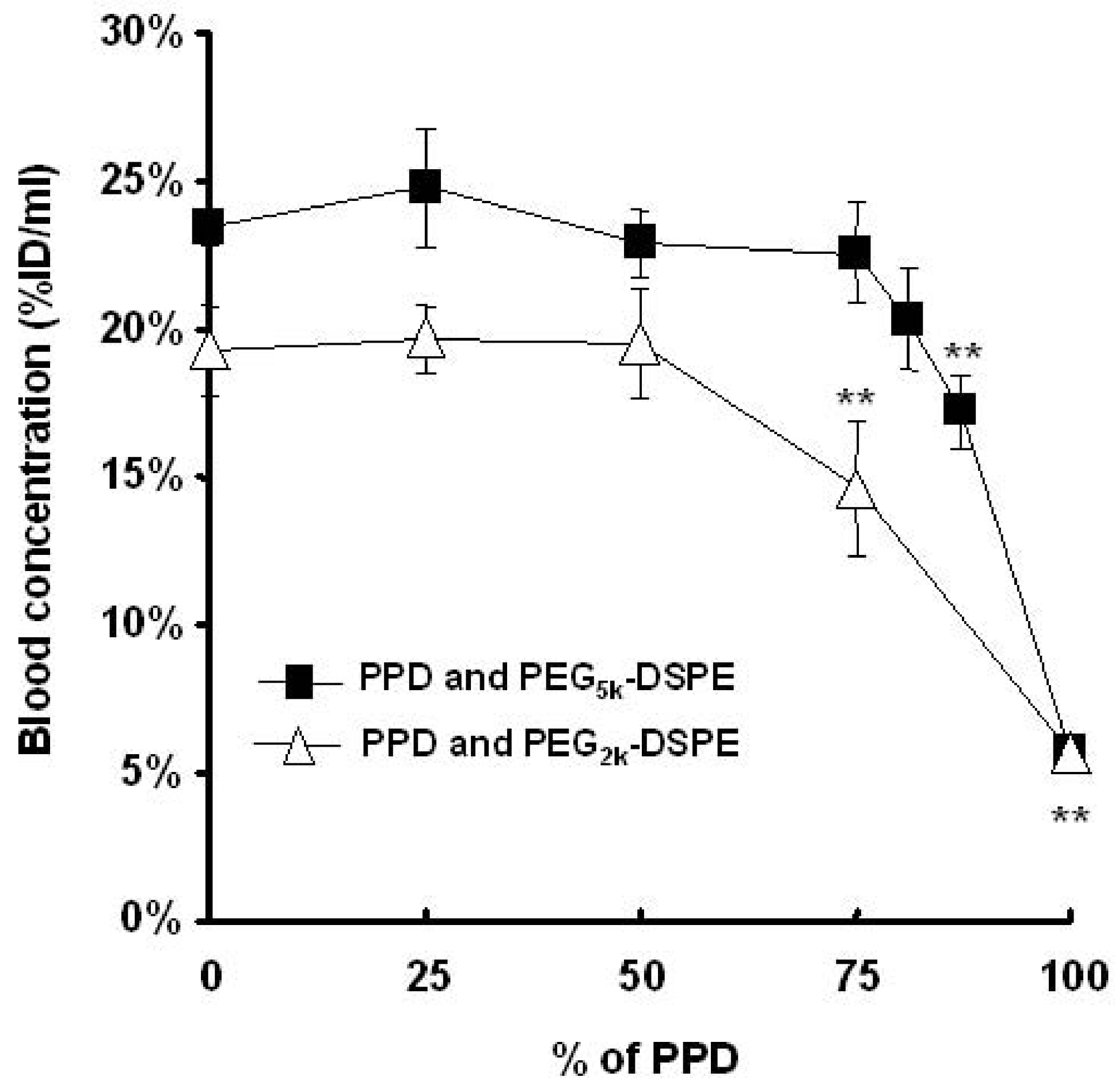
30%
25%
20%
15%
10%
5%
0%
Blood concentration (%ID/ml)
PPD and PEG5k-DSPE
PPD and PEG2k-DSPE
**
**
**
0
25
50
75
100
% of PPD

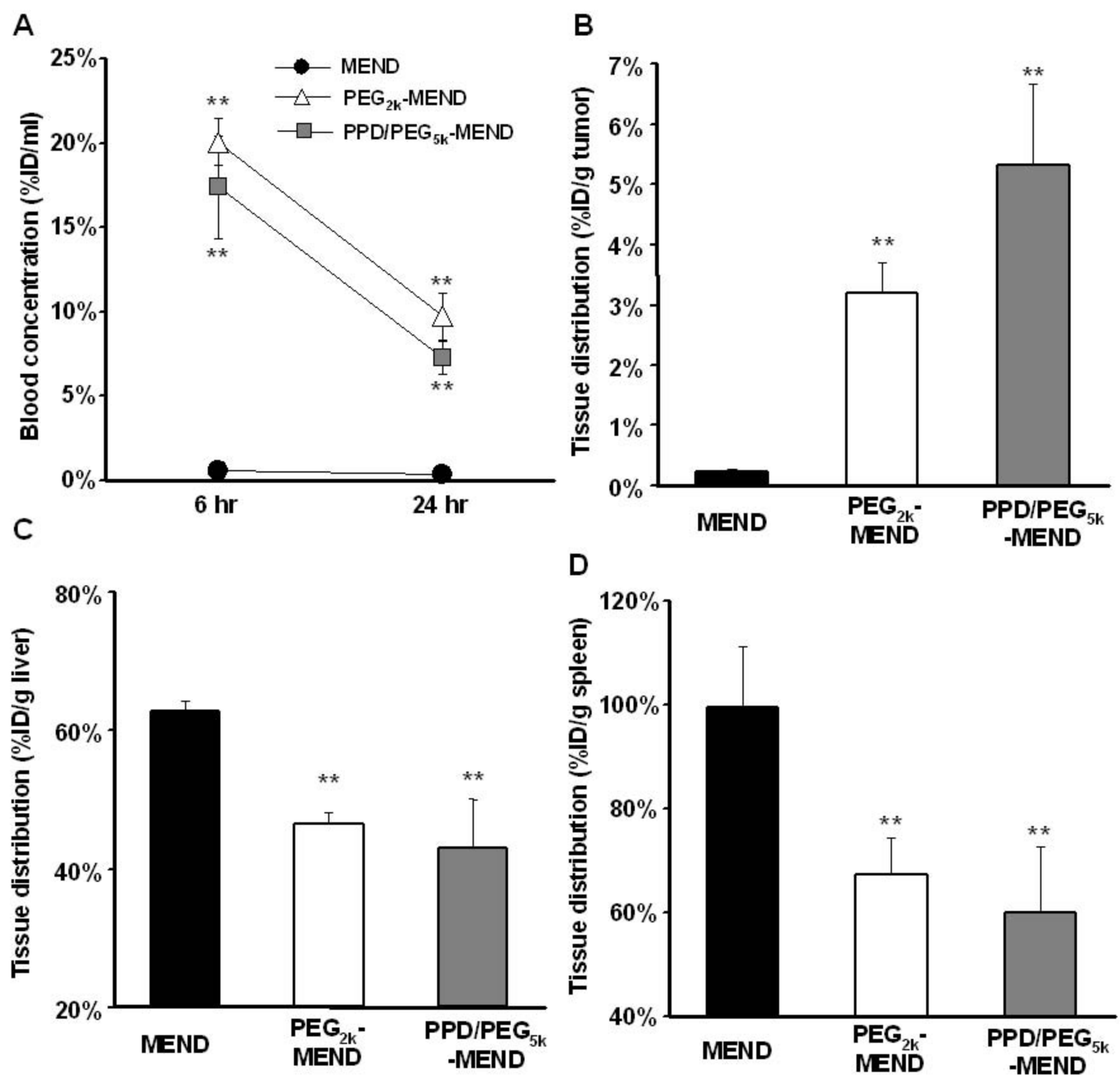
A
25%
20%
15%
10%
5%
0%
Blood concentration (%ID/ml)
MEND
PEG2k-MEND
PPD/PEG5k-MEND
**
6 hr
24 hr
B
7%
6%
5%
4%
3%
2%
1%
0%
Tissue distribution (%ID/g tumor)
MEND
PEG2k-MEND
PPD/PEG5k-MEND
C
80%
60%
40%
20%
Tissue distribution (%ID/g liver)
D
120%
100%
80%
60%
40%
Tissue distribution (%ID/g spleen)

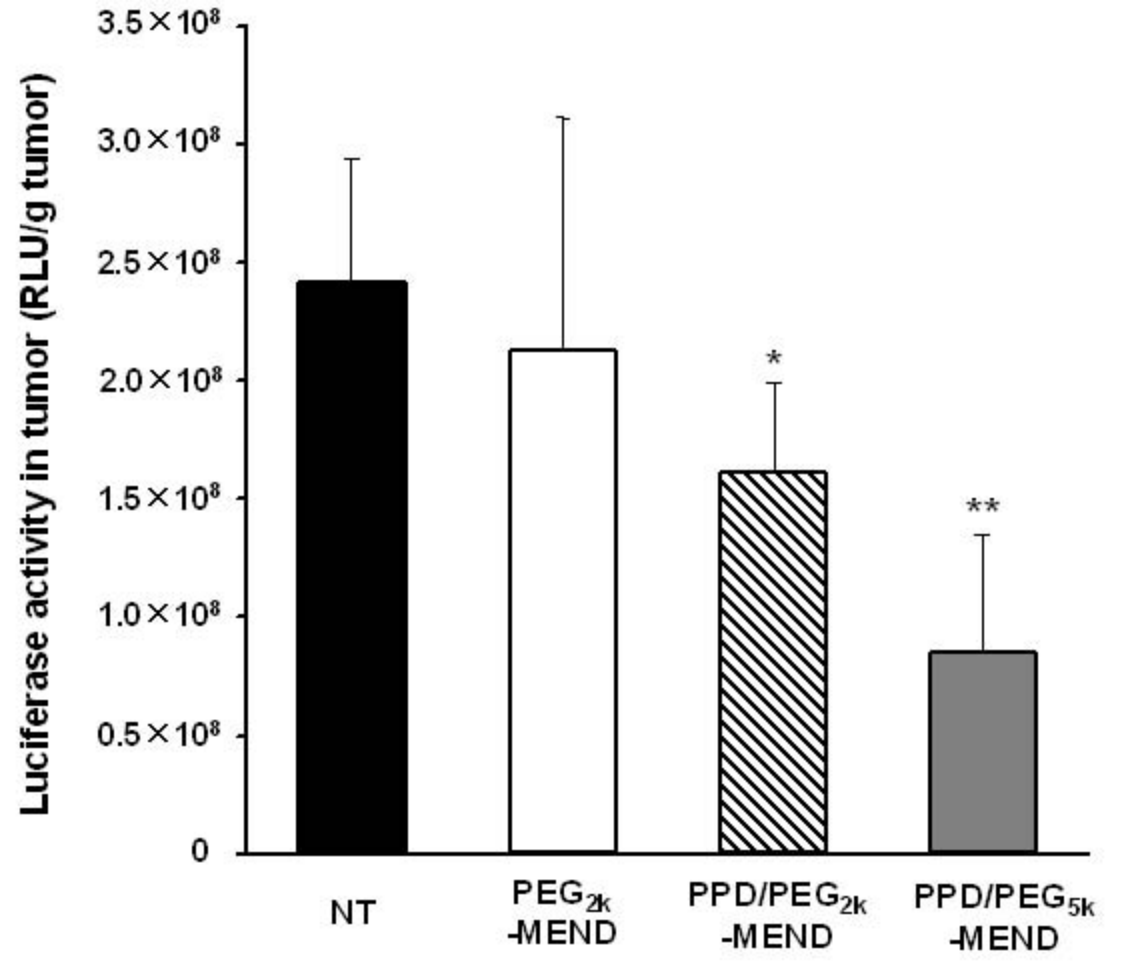
Luciferase activity in tumor (RLU/g tumor)
3.5×10^8
3.0×10^8
2.5×10^8
2.0×10^8
1.5×10^8
1.0×10^8
0.5×10^8
0
*
**
NT
PEG2k -MEND
PPD/PEG2k -MEND
PPD/PEG5k -MEND

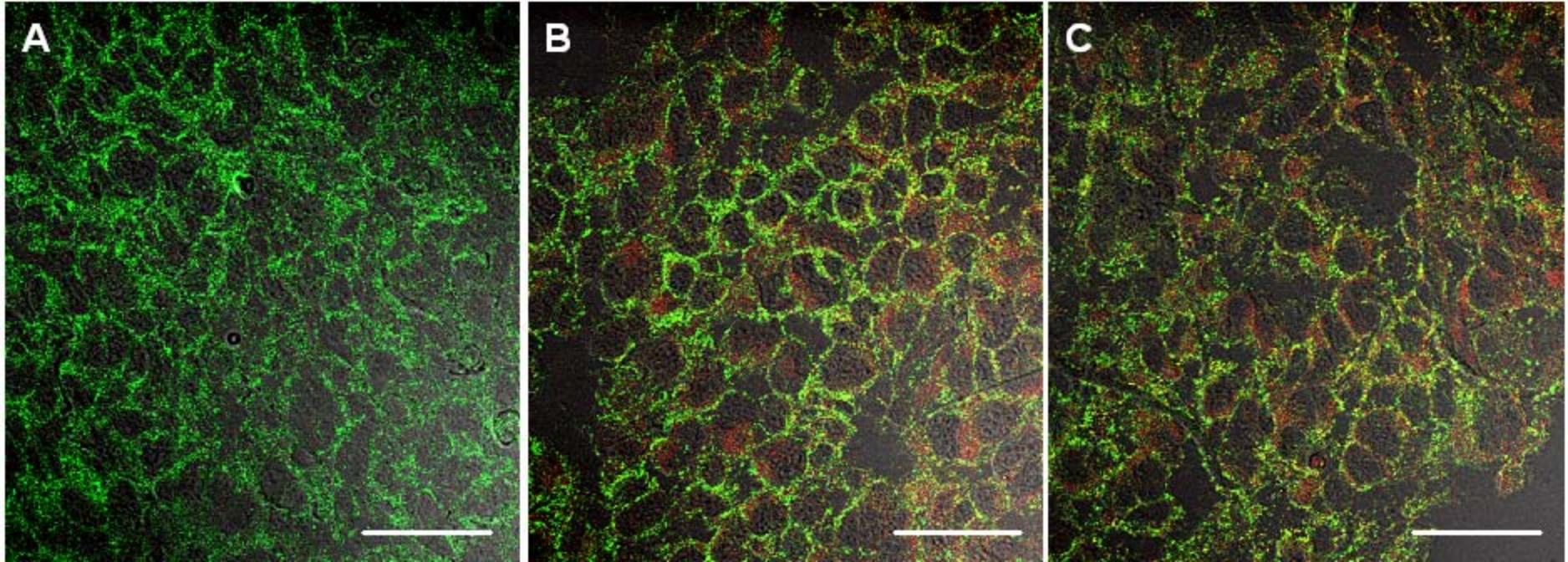
A
B
C

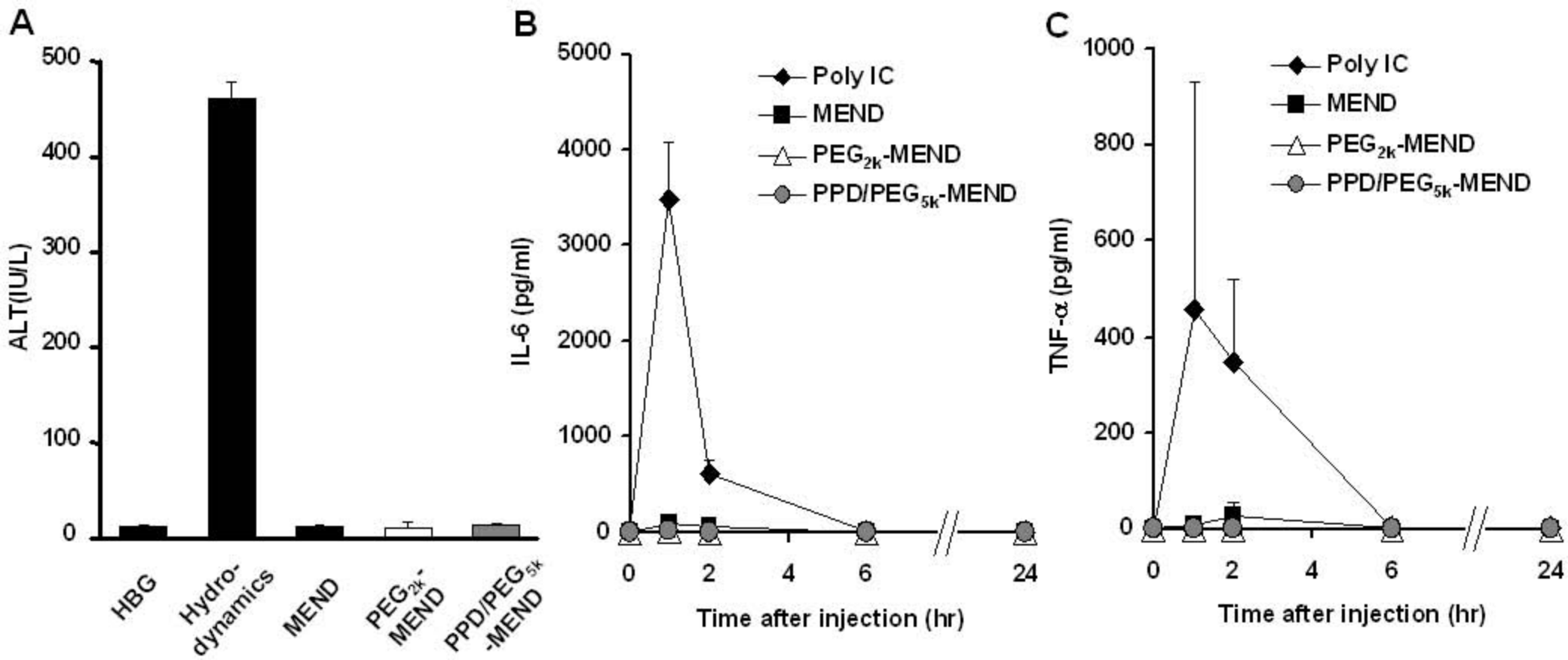
A
ALT(IU/L)
500
400
300
200
100
0
HBG
Hydro-dynamics
MEND
PEG2k-MEND
PPD/PEG5k-MEND
B
IL-6 (pg/ml)
5000
4000
3000
2000
1000
0
Poly IC
MEND
PEG2k-MEND
PPD/PEG5k-MEND
0
2
4
6
24
Time after injection (hr)
C
TNF-α (pg/ml)
1000
800
600
400
200
0
Poly IC
MEND
PEG2k-MEND
PPD/PEG5k-MEND
0
2
4
6
24
Time after injection (hr)

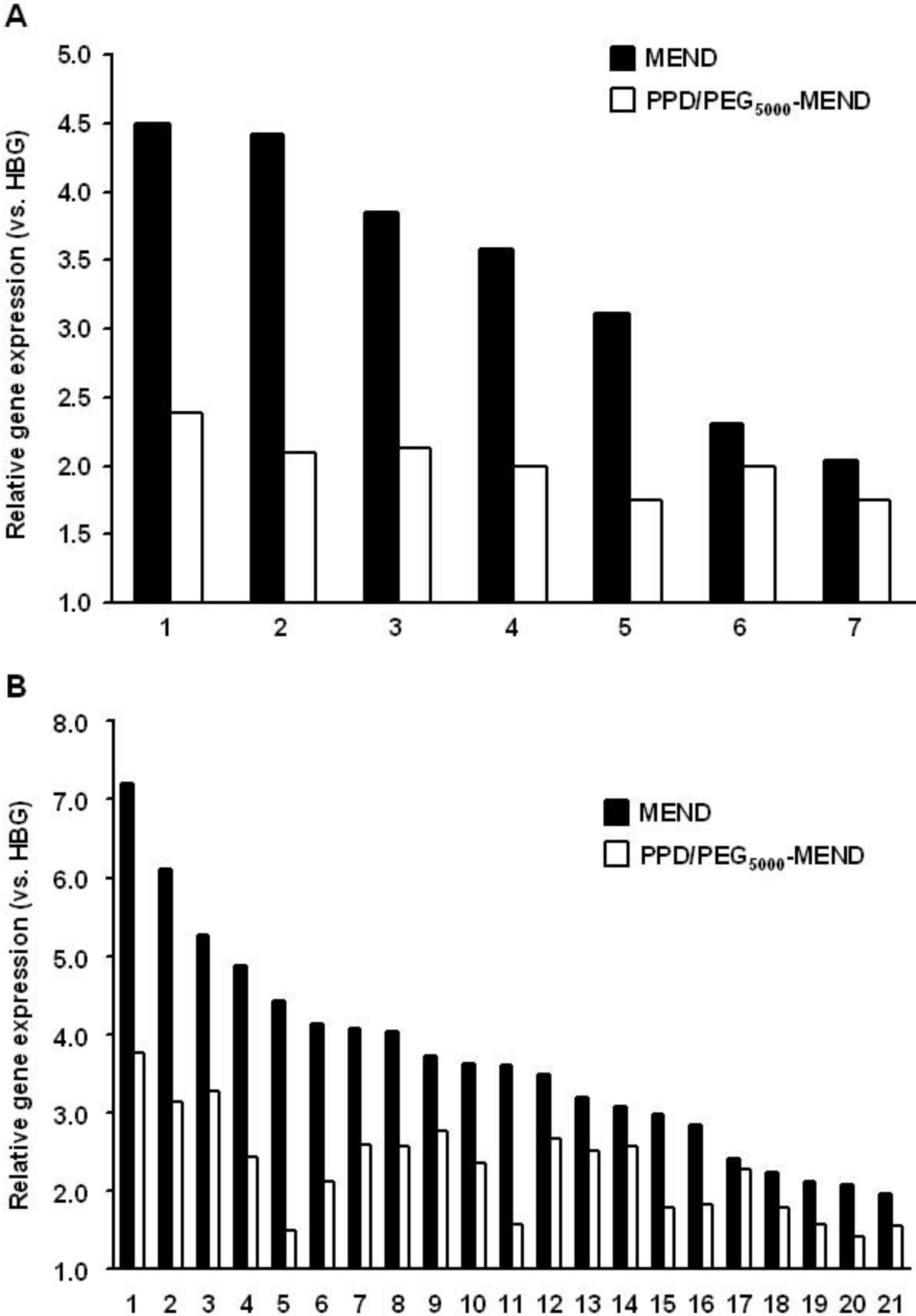
A
MEND
PPD/PEG5000-MEND
Relative gene expression (vs. HBG)
5.0
4.5
4.0
3.5
3.0
2.5
2.0
1.5
1.0
1
2
3
4
5
6
7
B
MEND
PPD/PEG5000-MEND
Relative gene expression (vs. HBG)
8.0
7.0
6.0
5.0
4.0
3.0
2.0
1.0
1 2 3 4 5 6 7 8 9 10 11 12 13 14 15 16 17 18 19 20 21

**Table 1 Characteristics of PEG-unmodified MEND and 5 mol% PEGylated MENDs for use in in vitro experiments**

| Fromulation | Diameter (nm) | ζ-potential (mV) |
|---|---|---|
| **MEND** | **190** | **37.8** |
| **PEG-MEND** | **117** | **1.8** |
| **PPD-MEND** | **134** | **3.2** |

MEND, PEG-MEND and PPD-MEND represents PEG-unmodified MEND, MEND modified with 5 mol% $PEG_{2k}$-DSPE and MEDN modified with 5 mol% PPD, respectively.

**Table 2 Characteristics of MENDs modified with 15 mol% PEG-lipid for use in in vivo experiments**

| Proportion of PEG-lipid (%) | | Diameter (nm) | ζ-potential (mV) |
|---|---|---|---|
| $PEG_{2k}$-DSPE | PPD | | |
| 100 | 0 | 94 | -9.8 |
| 75 | 25 | 91 | -9.3 |
| 50 | 50 | 89 | -11.2 |
| 25 | 75 | 107 | -8.8 |
| 0 | 100 | 115 | -11.6 |
| $PEG_{5k}$-DSPE | PPD | | |
| 100 | 0 | 81 | -8.8 |
| 75 | 25 | 94 | -7.4 |
| 50 | 50 | 102 | -5.1 |
| 25 | 75 | 111 | -6.5 |
| 18.75 | 81.25 | 106 | -7.0 |
| 12.5 | 87.5 | 106 | -7.4 |

**Table 3 Genes that are differentially expressed in response to MEND and PPD/PEG$_{5k}$-MEND treatment in liver and spleen by a DNA microarray**

**Liver**

| No | Genebank | Discription | Ratio | | |
|---|---|---|---|---|---|
| | | | MEND/HBG | PEGylated MEND /HBG | PEGylated MEND /MEND |
| 1 | NM_010479 | heat shock protein 1A (Hspa1a) | 4.50 | 2.39 | 0.53 |
| 2 | NM_015783 | interferon, alpha-inducible protein (G1p2) | 4.41 | 2.09 | 0.47 |
| 3 | NM_010479 | heat shock protein 1A (Hspa1a) | 3.84 | 2.12 | 0.55 |
| 4 | NM_011854 | 2'-5' oligoadenylate synthetase-like 2 (Oasl2) | 3.59 | 1.99 | 0.55 |
| 5 | NM_010501 | interferon-induced protein with tetratricopeptide repeats 3 (Ifit3) | 3.11 | 1.75 | 0.56 |
| 6 | NM_011940 | interferon activated gene 202B (Ifi202b) | 2.31 | 1.99 | 0.86 |
| 7 | NM_008329 | interferon, gamma-inducible protein 16 (Ifi16) | 2.04 | 1.76 | 0.86 |

**Spleen**

| No | Genebank | Discription | Ratio | | |
|---|---|---|---|---|---|
| | | | MEND/HBG | PEGylated MEND /HBG | PEGylated MEND /MEND |
| 1 | NM_008331 | interferon-induced protein with tetratricopeptide repeats 1 (Ifit1) | 7.20 | 3.76 | 0.52 |
| 2 | NM_145227 | 2'-5' oligoadenylate synthetase 2 (Oas2) | 6.11 | 3.13 | 0.51 |
| 3 | NM_015783 | interferon, alpha-inducible protein (G1p2) | 5.26 | 3.28 | 0.62 |
| 4 | NM_008332 | interferon-induced protein with tetratricopeptide repeats 2 (Ifit2) | 4.87 | 2.43 | 0.50 |
| 5 | NM_010479 | heat shock protein 1A (Hspa1a) | 4.43 | 1.51 | 0.34 |
| 6 | XM_129595 | similar to Ifi204 protein | 4.14 | 2.12 | 0.51 |
| 7 | NM_011854 | 2'-5' oligoadenylate synthetase-like 2 (Oasl2) | 4.07 | 2.59 | 0.64 |
| 8 | NM_011940 | interferon activated gene 202B (Ifi202b) | 4.03 | 2.57 | 0.64 |
| 9 | NM_145209 | 2'-5' oligoadenylate synthetase-like 1 (Oasl1) | 3.71 | 2.76 | 0.74 |
| 10 | NM_016850 | interferon regulatory factor 7 (Irf7) | 3.62 | 2.34 | 0.65 |
| 11 | NM_010479 | heat shock protein 1A (Hspa1a) | 3.59 | 1.57 | 0.44 |
| 12 | NM_145153 | 2'-5' oligoadenylate synthetase 1F (Oas1f) | 3.48 | 2.66 | 0.76 |
| 13 | NM_145211 | 2'-5' oligoadenylate synthetase 1A (Oas1a) | 3.18 | 2.51 | 0.79 |
| 14 | NM_010501 | interferon-induced protein with tetratricopeptide repeats 3 (Ifit3) | 3.08 | 2.57 | 0.83 |
| 15 | NM_027835 | interferon induced with helicase C domain 1 (Ifih1) | 2.98 | 1.78 | 0.60 |
| 16 | NM_008329 | interferon, gamma-inducible protein 16 (Ifi16) | 2.85 | 1.83 | 0.64 |
| 17 | NM_011163 | protein kinase, interferon-inducible double stranded RNA dependent (Prkr) | 2.41 | 2.29 | 0.95 |
| 18 | NM_145226 | 2'-5' oligoadenylate synthetase 3 (Oas3) | 2.23 | 1.78 | 0.80 |
| 19 | NM_013559 | heat shock protein 105 (Hsp105) | 2.12 | 1.56 | 0.74 |
| 20 | NM_008326 | interferon inducible protein 1 (Ifi1) | 2.08 | 1.42 | 0.69 |
| 21 | NM_027320 | interferon-induced protein 35 (Ifi35) | 1.97 | 1.55 | 0.79 |